

Polymer-Coated Echogenic Lipid Nanoparticles with Dual Release Triggers

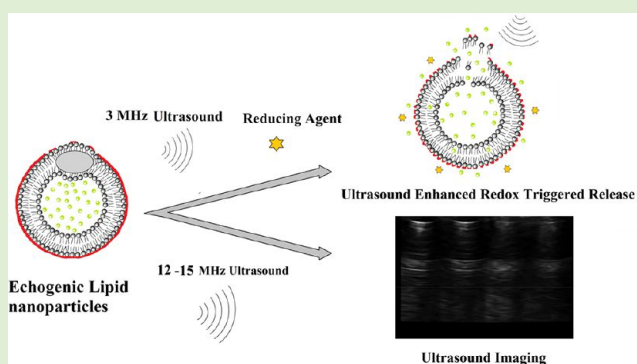
Rahul Nahire,[†] Manas K. Haldar,[†] Shirshendu Paul,[‡] Anaas Mergoum,[†] Avinash H. Ambre,[§] Kalpana S. Katti,[§] Kara N. Gange,^{||} D. K. Srivastava,[⊥] Kausik Sarkar,^{‡,#} and Sanku Mallik^{*,†}

Departments of [†]Pharmaceutical Sciences, [⊥]Chemistry and Biochemistry, [§]Civil Engineering, and ^{||}Health, Nutrition and Exercise Sciences, North Dakota State University, Fargo, North Dakota 58108, United States

[‡]Department of Mechanical Engineering, University of Delaware, Newark, Delaware 19716, United States

[#]Department of Mechanical and Aerospace Engineering, George Washington University, Washington, District of Columbia 20052

ABSTRACT: Although lipid nanoparticles are promising drug delivery vehicles, passive release of encapsulated contents at the target site is often slow. Herein, we report contents release from targeted, polymer-coated, echogenic lipid nanoparticles in the cell cytoplasm by redox trigger and simultaneously enhanced by diagnostic frequency ultrasound. The lipid nanoparticles were polymerized on the external leaflet using a disulfide cross-linker. In the presence of cytosolic concentrations of glutathione, the lipid nanoparticles released 76% of encapsulated contents. Plasma concentrations of glutathione failed to release the encapsulated contents. Application of 3 MHz ultrasound for 2 min simultaneously with the reducing agent enhanced the release to 96%. Folic acid conjugated, doxorubicin-loaded nanoparticles showed enhanced uptake and higher cytotoxicity in cancer cells overexpressing the folate receptor (compared to the control). With further developments, these lipid nanoparticles have the potential to be used as multimodal nanocarriers for simultaneous targeted drug delivery and ultrasound imaging.



INTRODUCTION

Targeted drug delivery remains one of the major challenges in current pharmaceutical research. Upon injection, many drugs get distributed in the body according to their pharmacokinetic and pharmacodynamic properties, resulting in low therapeutic concentrations at the target site and unwanted side effects. The drug biodistribution can be suitably altered and side effects can be minimized by employing targeted delivery systems. A wide variety of drug carriers and passive and active targeting strategies have been reported in the literature.¹ However, upon reaching the intended site, the rate of drug release from the carriers is often very slow. For example, one of the marketed liposomal doxorubicin formulations (Doxil) is passively targeted to the tumors employing the enhanced permeation and retention (EPR) effect.² Because of its long circulation time and slow drug release kinetics, several side effects of Doxil are reported (e.g., hand-foot syndrome, neutropenia, anemia, and thrombocytopenia).³

Stimuli-responsive drug delivery vehicles are highly attractive because of local control over payload release and, consequently, reduced systemic toxicity. Both biological/endogenous (e.g., enzymes,^{4,5} redox,⁶ and pH⁷) and nonbiological/exogenous (e.g., temperature,⁸ light,⁹ and ultrasound¹⁰) triggers have been used as stimuli to release the payload of these drug carriers. A combination of a biological and an external trigger can give dual levels of control for drug release at the targeted site.

Incorporation of concurrent contrast imaging capability renders multimodal characteristics to the drug carrier. However, there are only a few reports of such multimodal nanocarriers responding to multiple triggering stimuli with simultaneous imaging capability.¹¹

Ultrasound has been extensively used as a tool for different applications using different carriers such as polymers,¹² micelles,¹³ emulsions,¹⁴ microcapsules,¹⁵ microspheres,¹⁶ and liposomes.¹⁷ Most of these reported applications use low frequency ultrasound (LFUS).^{18–26} Although application of kHz frequency ultrasound leads to more release compared to MHz²⁰ frequency, it has very limited clinical applications due to the associated harmful biological effects. There are only a few reports of MHz frequency ultrasound utilized to release drugs from liposomes^{10,27–30} and microbubbles conjugated to liposomes.³¹

Acoustically reflective lipid nanoparticles/liposomes (echogenic liposomes or ELIPs) have been developed as stimuli-responsive drug carriers.^{32,33} The ELIPs are prepared in the presence of a cryoprotectant (e.g., mannitol) that helps in entrapping air pockets within the liposomes and thereby making them responsive to acoustic excitation. Ever since the

Received: December 10, 2012

Revised: January 26, 2013

Published: February 8, 2013

first report³⁴ of acoustically reflective liposomes, questions are raised on the presence and the exact location of entrapped air, especially when the diameters of the vesicles are small ($<1 \mu\text{m}$). Consequently, different terms are currently used for this system, for example, lipid nanoparticles, lipid dispersions, bubble liposomes,^{17,35,36} acoustically reflective liposomes,³⁷ and echogenic liposomes.³⁸ Although termed differently, these systems are fundamentally acoustically reflective lipid nanoparticles (ARLINS), as these are made of phospholipids and are in nanometer dimensions. Thus, we will refer to these lipid particles as ARLINS in this manuscript. Although the exact location of the entrapped air in ARLINS remains uncertain^{33,39–41} their echogenic properties have been well established through comprehensive acoustic experiments.^{41–43} The ARLINS are being studied as novel ultrasound imaging contrast agents for atherosclerotic plaques and cancerous tumors.⁴² Extensive ultrasound-mediated drug release studies^{27,39,44} with ARLINS have established their potential as simultaneous drug delivery and ultrasound imaging agents.

The lipid-based drug delivery systems offer excellent biocompatible vehicles for both hydrophilic and lipophilic drugs. However, in the biological system, they get destabilized due to interactions with plasma proteins and biomembranes, resulting in leakage of the encapsulated drugs in the circulation (before reaching the intended site).⁴⁵ This could result in only a small fraction of drug actually reaching the targeted site. Polymerization of the lipid bilayer improves stability but their clinical usage is limited because of poor biocompatibility.

The tripeptide glutathione (*L*- γ -glutamyl-*L*-cysteinylglycine, GSH) functions as an important free radical scavenger and protects cells from harmful effects of reactive oxygen species, toxins, drugs, and many mutagens. It is one of the most abundant organic reducing agents present in the human body. GSH level is elevated in various human cancer tissues (such as breast,^{46,47} ovary,⁴⁶ colon,⁴⁸ lung,⁴⁹ bone marrow,⁵⁰ and larynx⁵¹) compared to normal tissues. It has been implicated in drug resistance and in tumor growth.⁵² The disulfide functional group has gained attention in the preparation of stimuli-responsive drug carriers because of its stability in mildly oxidizing environments (of atmospheric oxygen and bloodstream⁵³) and its lability in the presence of reducing agents. Due to the large redox potential difference between the extracellular matrix (thiol concentration: 10–40 μM) and the cytosol of cancer cells (thiol concentration: 0.5–10 mM because of the presence of GSH),⁵⁴ the reversible disulfide thiol conversion is being widely used for cytosolic drug delivery.^{55–58}

Herein, we have prepared folate conjugated, disulfide-cross-linked, polymer-coated, acoustically reflective lipid nanoparticles for cytosolic drug delivery. When exposed to mM concentration of reducing agents, these polymer-coated lipid nanoparticles release their contents and this release is further enhanced by applying diagnostic frequency ultrasound (3 MHz, 0.5 MPa, CW) for 2 min. We have also imaged these lipid nanoparticles by using diagnostic frequency ultrasound. With further developments, these polymerized lipid nanocarriers hold promise as a vehicle for ultrasound image guided, targeted cytosolic drug delivery. To the best of our knowledge, there are no reports of using polymer-coated acoustically reflective lipid nanoparticles for simultaneous targeted drug delivery and ultrasound imaging.

MATERIALS AND METHODS

Preparation and Polymerization of ARLINS. The gallate derivative with three propargyl groups coupled to 1-palmitoyl-2-oleoyl-*sn*-glycerol-3-phosphoethanolamine (POPE-G) was synthesized following a published procedure.⁵⁹ Stock solution of 1-palmitoyl-2-oleoyl-*sn*-glycerol-3-phosphocholine (POPC, Avanti Polar Lipids) was prepared (1 mg/mL) by dissolving the lipid powder in chloroform and methanol (9:1) and stored in freezer ($-20 \text{ }^\circ\text{C}$). Solutions of POPC (3 mg), POPE-G (3.9 mg), and 1,2-dipalmitoyl-*sn*-glycerol-3-phosphoethanolamine-*N*-[lissamine rhodamine B sulfonyl] ammonium salt (DPPE-LR, 0.045 mg) were mixed in the molar ratio of 50:49:1, respectively, in a 10 mL round-bottom flask. The mixture was swirled to ensure proper mixing of components. Solvent was evaporated using a rotary evaporator, and the flask was placed under vacuum overnight to remove any residual solvent traces. Next day, the dried film was hydrated for 3 h with 3 mL of 10 μM calcein dissolved in 10 mM HEPES buffer (pH adjusted to 7.4) and 3 mL of 0.64 M mannitol (final concentration 0.32 M). The lipid dispersion was then bath sonicated for 10 min with constant swirling and exposed to three freeze ($-70 \text{ }^\circ\text{C}$) and thaw ($23 \text{ }^\circ\text{C}$) cycles to enhance calcein encapsulation. Sequential extrusion was performed using a mini-extruder (Avanti Polar Lipids) using 800 nm and 200 nm polycarbonate filters (Nuclepore, Whatman) in succession.

For cancer cell uptake studies, ARLINS were prepared using the same protocol, except that the concentration of calcein used was 3 mM. Two different batches were prepared, one with and the other without (1 mol %, 0.1 mg) 1,2-distearoyl-*sn*-glycerol-3-phosphoethanolamine-*N*-[folate(polyethylene glycol)-2000] (ammonium salt).

For polymerization, the reported procedure⁵⁹ was modified in order to make it suitable for our experiments. To the above 6 mL solution, the cross-linker CL (150 μL of 0.04 M aqueous solution), Cu²⁺ complex (150 μL of 0.053 M aqueous solution prepared by mixing 3 mL of CuCl₂, 71.7 mg, 0.53 mmol) solution, 3 mL of PMDETA solution (442 μL , 2.1 mmol), and sodium ascorbate (150 μL of 27 mg/mL solution, 1.4 μmol) were added together. The mixture was divided into six closed vials and stirred slowly at room temperature for 24 h. After 24 h, the mixture was passed through a Sephadex-G100 gel (GE healthcare) filtration column in order to remove unencapsulated dye and other compounds from the ARLINS. Mannitol was added to the ARLINS solution to obtain 0.32 M concentration, the solution was frozen, and subsequently, the ARLINS were placed in a lyophilizer. The freeze-dried powder was stored in a refrigerator and reconstituted just before use.

Preparation of Doxorubicin-Loaded ARLINS. To encapsulate doxorubicin into the lipid nanoparticles, the reported pH gradient loading method was employed⁶⁰ with some modifications. Briefly, the lipid film was hydrated with 400 mM citrate buffer (pH 4). After bath sonication and freeze thaw cycles, the external pH of buffer increased to 7.4 by the addition of dilute sodium hydroxide. To this lipid dispersion, 0.2 mg of doxorubicin/mg of lipid was added and the dispersion was stirred for 30 min at room temperature. The lipid dispersion was then passed through a Sephadex-G100 gel filtration column to remove unencapsulated doxorubicin. Encapsulation efficiency was determined by recording the absorbance of doxorubicin at 475 nm before and after gel filtration. These lipid nanoparticles were then polymerized using the same procedure described earlier. After polymerization, the doxorubicin content was determined by plotting the absorbance onto the calibration curve established at 475 nm.

Measurement of Size Distribution, Zeta Potential, and Mobility. The size distribution, zeta potential, and mobility of the ARLINS were measured by Malvern Zetasizer Nano-ZS90 using dynamic light scattering (DLS) method before and after lyophilization. Polystyrene latex disposable cuvettes (DTS 0012 for size and DTS 1061 for zeta potential and mobility) were used, and scattering measurement was performed at a 90° angle. Each sample (0.1 mg/mL in 10 mM HEPES buffer pH 7.4) was equilibrated for 60 s and 10 readings were taken for each sample of ARLINS at room temperature. All the batches were tested and each sample was tested five times to ensure reproducibility and to calculate the standard deviation.

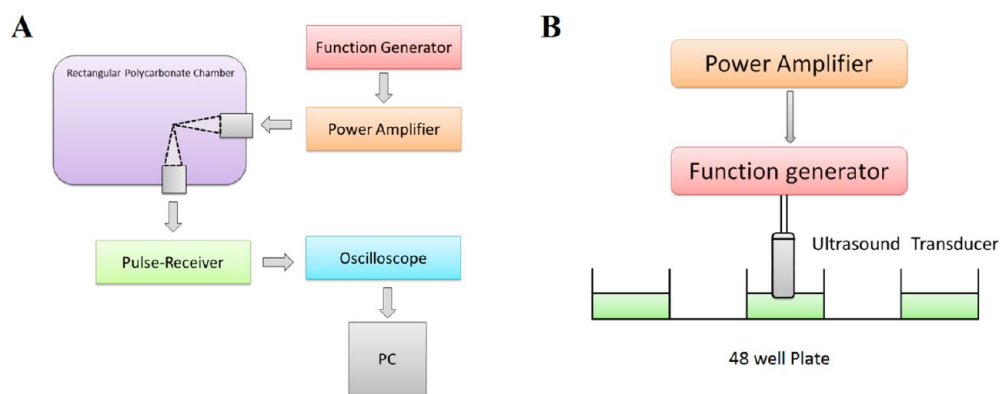


Figure 1. (A) Schematic of the experimental setup for in vitro measurement of scattering. (B) Schematic of the in vitro experimental setup for ultrasound mediated release studies.

Transmission Electron Microscopy. The samples were observed using a JEOL JEM-2100-LaB₆ transmission electron microscope operating at 200 kV at low magnifications and with the beam spread, which is not converged, to reduce the amount of electron beam interaction per unit area and, hence, beam damage to sample if it were to occur. Lyophilized ARLINs sample reconstituted in 10 mM HEPES buffer pH 7.4 to obtain 1 mg/mL concentration and dropped onto 300 mesh Formvar-coated copper grids previously coated with 0.01% poly-L-lysine and allowed to stand for a minute before wicking off with filter paper. After air drying for 2 min, the sample was negatively stained with 1% phosphotungstic acid for 1.5 min and subsequently wicked off with filter paper and allowed to dry before viewing.

Atomic Force Microscopy (AFM). The sample (freshly reconstituted in 10 mM HEPES buffer pH 7.4) was dropped onto a mica sheet and air-dried for performing the AFM experiments. For performing AFM imaging, a Multimode atomic force microscope with Nanoscope III a controller and J type piezo scanner from Veeco Metrology Group, Santa Barbara, CA, was used. Antimony (n) doped Si tip was used for obtaining images in tapping mode under laboratory conditions. Images were taken before and after treatment with 5 mM GSH.

Measurement of Echogenicity of ARLINs. Echogenicity of the ARLINs was measured in vitro using the acoustic setup to measure scattered response discussed in our previous publications⁴¹ (Figure 1A). The setup consisted of two single element focused immersion transducers (Panametrics-NDT) confocally positioned at right angles by inserting them through holes drilled on the adjacent walls of a rectangular polycarbonate chamber that held our sample volume. Each transducer had an individual diameter of 1.27 cm with a focal length of 3 cm. The transmitting and receiving transducers had nominal central frequencies of 3.87 and 5.54 MHz and -6 dB bandwidths of 86.4 and 85%, respectively. A programmable function generator (Model 3325A; Agilent Santa Clara, CA) was used to generate a 32 cycle sinusoidal wave at 3.5 MHz frequency, which was then amplified using a power amplifier (Model A-300; ENI, Rochester, NY) before being fed to the transmitting transducer. The output of the transducer was calibrated using a needle hydrophone (PZT-Z44-0400, Onda Corporation, CA). All scattering experiments were performed at an acoustic pressure of 500 kPa. The scattered signal was received through a pulser/receiver (Model 5800; Panametrics-NDT, Waltham, MA) with a 20 dB gain. The received signal was observed in real-time utilizing a digital oscilloscope (Model TDS2012; Tektronix, Beaverton, OR). Scattered voltage–time responses were saved on a desktop computer for postexperimental analysis using LabView (Version 6.0.3; National Instruments, Austin, TX) connected to the oscilloscope via a GPIB IEEE 488 cable and GPIB card. The voltage–time responses were analyzed using a Matlab code (MathWorks, Natick, MA) by taking Fast Fourier Transforms of 50 oscilloscope acquisitions, which were averaged and converted to dB scale with unit reference before extracting the responses at desired frequencies (fundamental, second, and subharmonics). Each experiment was repeated five times and the

average responses with corresponding standard deviation errors were plotted.

Phosphate buffered saline (PBS) solution mixed with 0.5% by weight of bovine serum albumin (BSA) were prepared and kept refrigerated for a minimum of 48 h before using them to reconstitute the freeze-dried ARLINs. Correct amounts of ARLINs were weighed and dissolved in 100 mL of PBS-BSA solution and poured into the sample chamber to carry out the scattering measurements. At the lipid concentration 5 $\mu\text{g}/\text{mL}$, it was sufficiently diluted so that multiple scattering could be safely neglected.

Ultrasound Imaging of ARLINs. Terason t3200 Diagnostic Ultrasound (MedCorp LLC., Tampa, FL) was used to image reconstituted ARLINs. A layer of Aquasonic 100 (Parker Laboratories, Inc., Fairfield, New Jersey) ultrasound gel was applied to the 15L4 Linear (4.0–15.0 MHz; MedCorp LLC., Tampa, FL) ultrasound transducer sound plate. The transducer with gel was placed over the parafilm covering the wells containing the ARLINs in a 96-well plate. The ultrasound scan properties of the ARLINs were set at 0.7 Mechanical Index (MI), 0.6 Thermal Index (TIS), Omni Beam activated, level C Image Map, level 3 Persistence, high (H) frequency, level 3 TeraVision, level 51 2D Gain, level 60 Dynamic Range (DR), 3 cm scan depth, and 22 Hz frame rate. The images were labeled and saved.

Ultrasound (US)-Mediated Release Studies. For US-mediated release studies with ARLINs, we used a setup similar to the one described in our previous publication⁴¹ (Figure 1B). A single element unfocused immersion transducer (Model IP301HP; Valpey Fisher Corporation, Hopkinton, MA) was used to excite the ARLINs suspension. Frequency (3 MHz) continuous sinusoidal waves utilized for the release studies were generated using the waveform generator (Model 33250A; Agilent, Santa Clara, CA) and amplified using a power amplifier (Model A-150; ENI, Rochester, NY) before being input to the transducer. The transducer output was calibrated using a needle hydrophone (PZT-Z44-0400, Onda Corporation, CA). All of our release studies with ultrasonic excitation were carried out at a pressure of 0.5 MPa with a 2 min exposure time. The release studies were performed in 48-well plates with a 500 μL sample volume and a lipid concentration of 0.02 mg/mL. The entire plate was placed on a constant temperature water bath to minimize temperature fluctuations and homogeneity of the sample was ensured by placing small magnetic stirrers within each well during the course of the experiment. Although this setup allows reflection of ultrasound wave from the air–water interface, thereby giving rise to standing wave patterns,^{61,62} the setup was found adequate for the present study to demonstrate the validity of the proof of concept. Also, as mentioned in our previous publication, we observed negligible (less than 1%) energy transfer to neighboring wells during stimulation indicating almost no interwell interference. All experiments were performed three times and in triplicate each time to ensure reproducibility of results and calculate standard deviations.

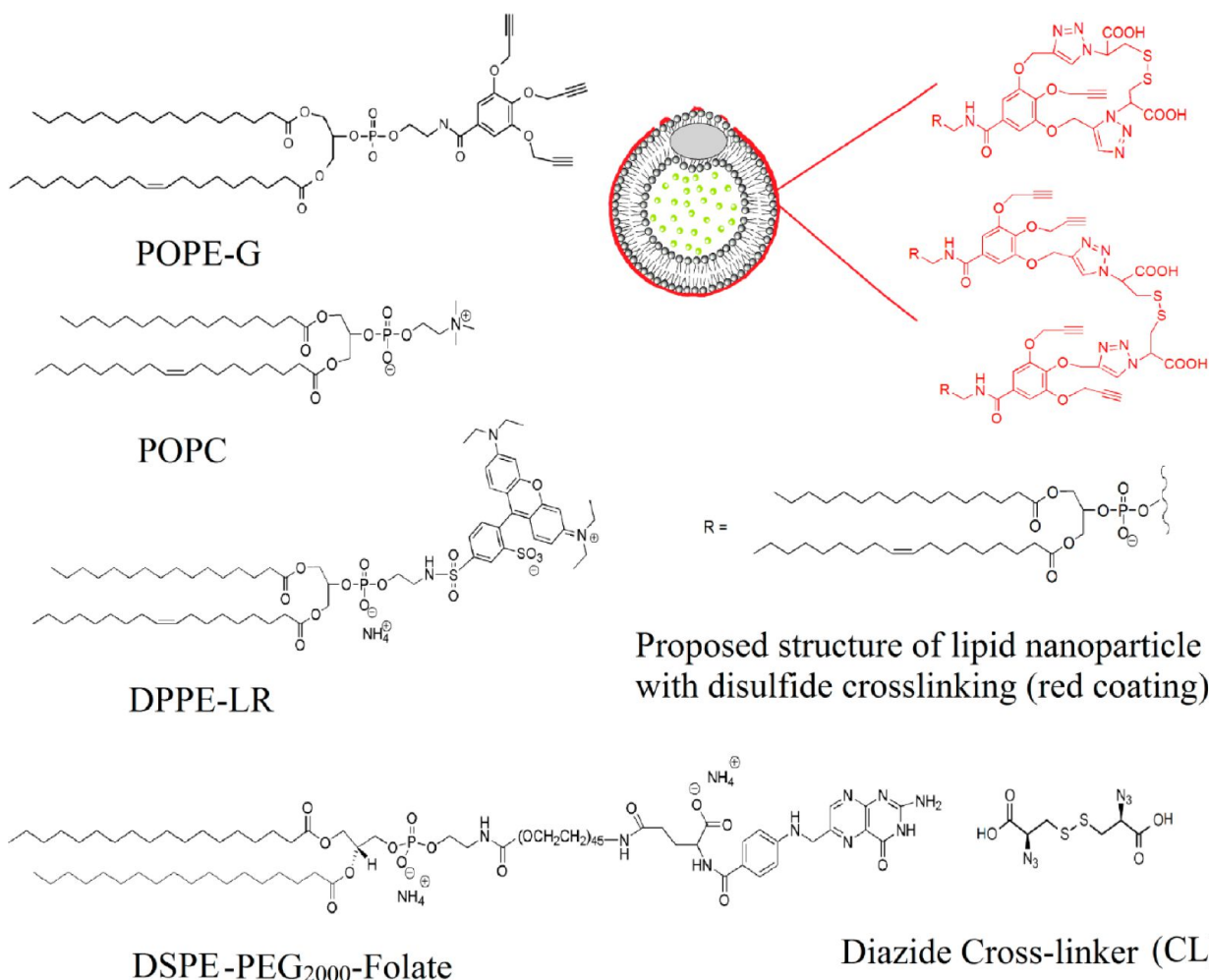


Figure 2. Lipids used in preparation of lipid nanoparticles and proposed structure of lipid nanoparticle with disulfide polymer coating (red coating around nanoparticle) after polymerization by diazide cross-linker CL.

Redox-Triggered Release Studies. Release studies were carried out using a fluorescence microplate multidetection instrument (Spectramax-M5, Molecular devices) using calcein and CoCl_2 quenching method. Since subself-quenching concentration ($10 \mu\text{M}$) of calcein was used, we could quench external fluorescence by adding CoCl_2 .^{10,27–30} CoCl_2 quenches fluorescence of unencapsulated calcein outside the ARLINs, so the fluorescence signal observed is from the encapsulated dye only. For the release studies, 0.02 mg/mL ARLINs were taken into 96-well plate and external calcein was quenched with 10 mM CoCl_2 . Dithiothreitol (DTT), glutathione (GSH), and cysteine (CYS) were added in specific concentration to determine the release of calcein. Fluorescence was monitored at 515 nm (excitation 495 nm) for an hour and, subsequently, the ARLINs were disrupted using triton-X100 to record background fluorescence (if any). Initial fluorescence intensity was treated as 100% and percent decrease in fluorescence intensity was treated as percent release accordingly.

$$\text{percent release} = \frac{\text{initial fluorescence} - \text{final fluorescence}}{\text{initial fluorescence}} \times 100$$

Ultrasound-Enhanced, Thiol-Triggered Release. For these experiments, a 48-well plate was used, in which 0.02 mg/mL of freeze-dried ARLINs were suspended in 10 mM HEPES buffer ($\text{pH} 7.4$). Two different set ups were employed to study the combined effects of reducing agents and ultrasound on release. In the first set up, ARLINs were incubated with 5 mM reducing agent and after 60 min, the solution was exposed to ultrasound (3 MHz , 0.53 MPa) for 2 min. In the second set up, we applied ultrasound immediately after the addition of the reducing agent. Control samples were kept and release

was checked for each experiment. Care was taken to keep two sample wells as far as possible to minimize the effect of ultrasound in other wells.

Cell Culture and ARLINs Uptake Studies. For cancer cell uptake studies, MCF-7 (human breast adenocarcinoma) and HeLa (human cervical carcinoma) cells were cultured in clear (without added Phenol Red) RPMI media supplemented with 10% fetal bovine serum and 1% antibiotics. The culture flasks were incubated at 37°C in humidified atmosphere containing 5% CO_2 . When cells became 90% confluent, they were suspended using trypsin-versene. The suspended cells then cultured onto sterile six-well plates until 90% confluent.

For uptake studies with calcein encapsulation, the media was removed and MCF-7 cells were gently washed with HBBS (Hank's Balanced Salt Solution) 2–3 times to completely remove any media. Subsequently, the ARLINs suspended in HBSS (0.2 mg/mL) were incubated with the cells for 30 min. After specific time intervals, ARLINs solution was removed from wells and cells were again rinsed with HBSS to remove ARLINs on the surface of cells. Hoechst-33342 stain (1 mg/mL , 1:1000 dilution) was used to stain nuclei of cells. Finally, fresh media was added to cells and were observed under fluorescent microscope at different time points (10, 20, and 30 min.). A similar procedure was followed for the uptake studies with doxorubicin-loaded ARLINs (targeted, nontargeted) using the HeLa cells.

Percent uptake of ARLINs by HeLa cells was calculated by measuring fluorescence of the cells lysed with 5% triton. For this, the cells were seeded onto a 96-well plate and, once confluent, incubated with ARLINs loaded with 50 mM calcein for 6 h at two different

concentrations (40 and 20 $\mu\text{g}/\text{mL}$). After incubation, the cells were washed with HBSS thrice and lysed using 5% triton-X100. The fluorescence was measured (Ex: 485 nm Em: 515 nm) and then compared with fluorescence of respective ARLINs solution lysed using 5% triton. Percent uptake was calculated for the folate targeted and nontargeted ARLINs at both concentrations.

Cell Viability Assay. The cytotoxicity of targeted and nontargeted ARLINs was determined by AlamarBlue assay, measuring the fluorescence of resorufin (red) formed by reduction of resazurin (blue) in the cytosol of viable cells (metabolically active).⁶³ Briefly, HeLa cells were transferred to flat, clear-bottomed, 96-well tissue culture plates (Corning) at a density of 2×10^4 per well 24 h prior to the assay (or 70–80% confluency). The culture medium in each well was carefully removed and replaced with doxorubicin-loaded folate-conjugated ARLINs, doxorubicin-loaded nontargeted ARLINs, and doxorubicin solution mixed with media. After incubation at 37 °C for 6, 12, and 24 h, the cells were washed three times with sterile HBSS and incubated in fresh culture medium. At this point, 20 μL of AlamarBlue was added to each well and the fluorescence readings (Ex: 560 nm Em: 590 nm) were taken after 3 h of incubation at 37 °C. Average readings were then compared with control and plotted on the graph.

RESULTS AND DISCUSSION

The gallate-derived polymerizable lipid (POPE-G) and the diazide cross-linker (CL) were synthesized in our laboratory. The lissamine rhodamine lipid (DPPE-LR) and the DSPE-PEG-2000-Folate are commercially available (Figure 2). We prepared the ARLINs incorporating 50 mol % POPC, 49 mol % POPE-G, and 1% DPPE-LR in 10 mM HEPES buffer (pH 7.4). Nanoparticles were polymerized in the presence of added diazide CL, CuSO_4 , and ascorbic acid and subsequently freeze-dried in the presence of a weak cryoprotectant mannitol. Based on a literature report, we anticipate that the disulfide cross-links were formed only on the outside surface of the lipid nanoparticles⁵⁹ (Figure 2). Being a weak cryoprotectant, mannitol does not provide effective protection during lyophilization, which leads to defects in the polymer-coated lipid shell. It has been hypothesized that these defects are responsible for the entrapment of air within the lipid nanoparticles during the rehydration/reconstitution stage.^{42,64} This entrapped air (which gives rise to mismatch of acoustic impedance) is critical for the echogenicity of these lipid structures. We have recently reported that a finite amount of mannitol is necessary during lyophilization for making them echogenic.⁴¹ We also observed that these lipid nanoparticles were echogenic, only when lyophilized and reconstituted; prior to freeze-drying, these were not echogenic, that is, did not respond to ultrasonic excitation. Hence, the polymerized ARLINs studied here were prepared using the freeze-drying technique mentioned above and tested for echogenicity.

We determined the size distribution of ARLINs before and after lyophilization using a dynamic light scattering (DLS) instrument. We observed that the number average diameter after lyophilization increased (117 ± 11 nm, Figure 3A) compared to the average diameter before lyophilization (78 ± 14 nm, Figure 3B). Polydispersity index was also found to increase from 0.37 ± 0.04 to 0.71 ± 0.05 , indicating a more heterogeneous distribution of sizes in the lyophilized sample. This was confirmed in subsequent transmission electron microscopic images obtained for lyophilized ARLINs (Figure 4B). Note that, due to the modified preparation protocol, the ARLINs indeed entrapped air, as verified by TEM images (Figure 4A), and gave rise to a more polydispersed suspension with a larger average diameter. We studied the effect of addition

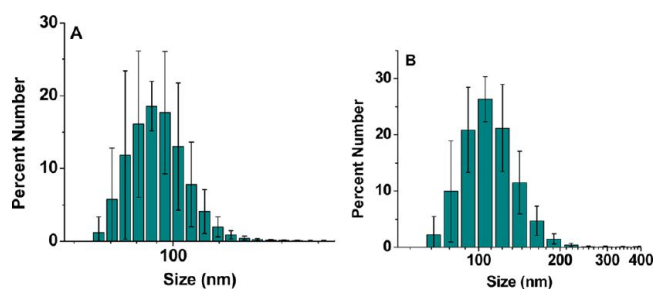


Figure 3. Size distribution analysis of nanoparticles by dynamic light scattering method. (A) Size distribution by number before lyophilization; (B) Size distribution by number after lyophilization ($n = 5$).

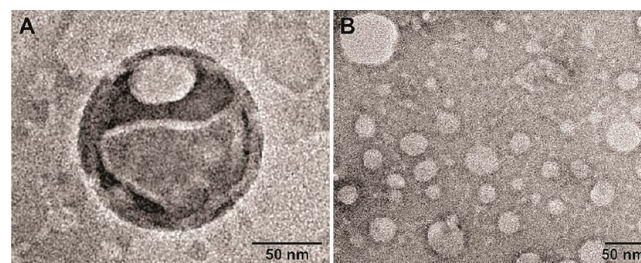


Figure 4. Transmission electron microscopic images of negatively stained ARLINs with 1% phosphotungstic acid, using a JEOL JEM-2100-LaB₆ transmission electron microscope operating at 200 kV. The beam is spread and not converged, to reduce the amount of electron beam interaction per unit area and to minimize beam damage to sample. (A) ARLINs after lyophilization showing presence of air bubble entrapped in the shell. (B) Heterogeneous size distribution of ARLINs after lyophilization.

of GSH on the morphology and size distribution of ARLINs, employing an atomic force microscope (AFM). We observed that, before treatment, ARLINs look spherical with average size about 100–200 nm (Figure 5A); but upon addition of 5 mM GSH, the particles fuse with each other and their size distribution becomes more heterogeneous (Figure 5B).

We also characterized these particles for their physical properties. We determined zeta potential and electrophoretic mobility of regular and doxorubicin encapsulated ARLINs using dynamic light scattering method employing the Zetasizer instrument (Table 1). During gel filtration with Sephadex column, the lipid particles may get adsorbed and thus their stability and physical characteristics may be changed. Hence, we compared the size, zeta potential, electrophoretic mobility, and stability of the ARLINs before and after gel filtration. We observed that gel filtration did not decrease stability of ARLINs as they leaked less than 5% of the encapsulated dye when incubated for an hour. We also noticed that gel filtration did not affect the physical characteristics of particles, for example, size, zeta potential, and electrophoretic mobility (Table 2).

Similar to other literature reports,^{34,65} we observed by TEM the presence of air bubble either inside the aqueous interior or in the shell of the ARLINs (Figure 4A). The ARLINs prepared following freeze-drying/reconstitution in the presence of mannitol also showed significant echogenicity, incontrovertibly indicating air entrapment. Figure 6 shows the scattered response from a suspension of ARLINs under ultrasonic excitation for two different frequency components, namely, fundamental (at frequency of excitation, 3.5 MHz) and second

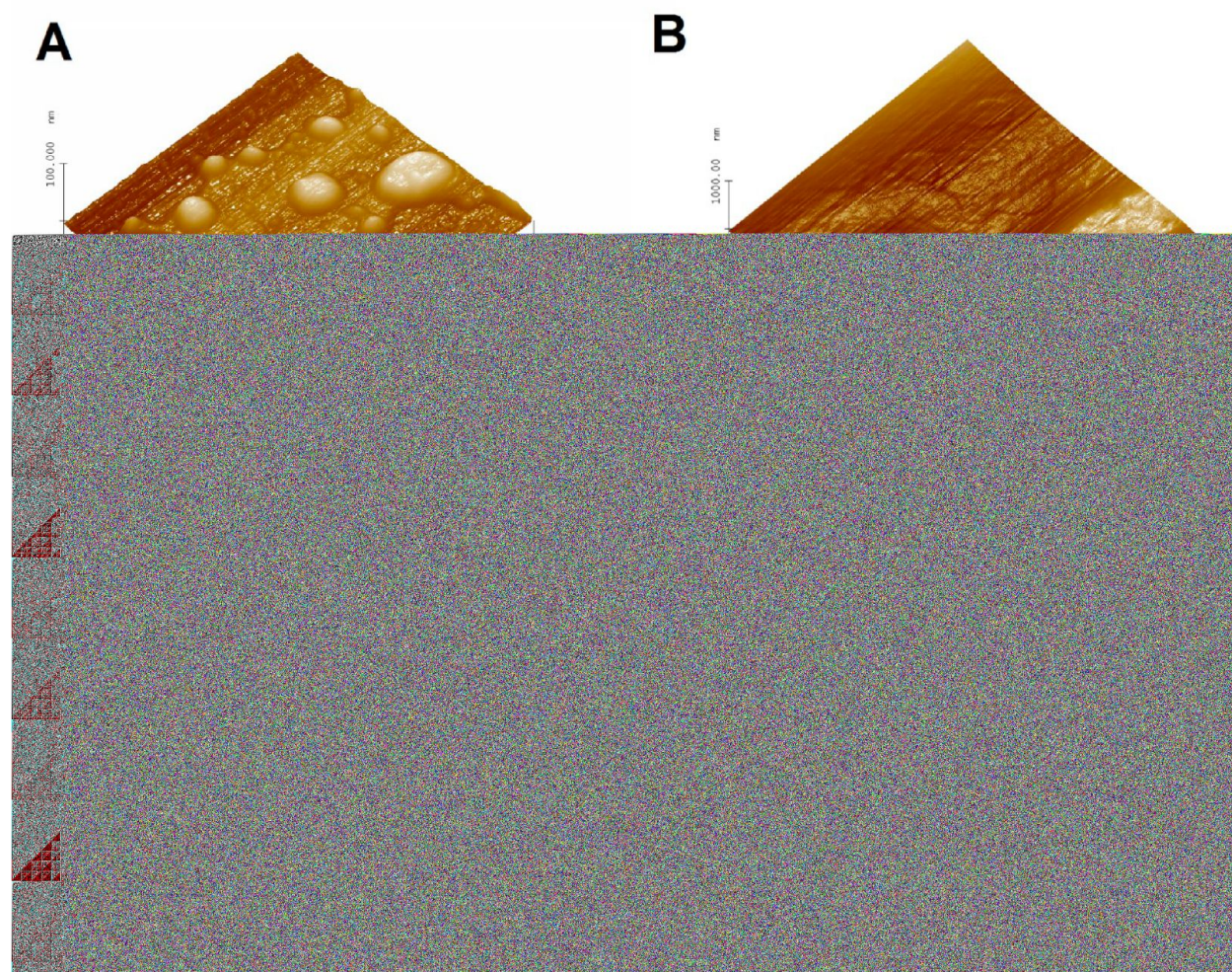


Figure 5. MultiMode atomic force microscopic images of ARLINs before (A) and after (B) treatment with 5 mM GSH.

Table 1. Zeta Potential and Electrophoretic Mobility of ARLINs and Doxorubicin-Encapsulated ARLINs Determined Using Dynamic Light Scattering Method ($n = 5$)

	zeta potential (mV)	electrophoretic mobility ($\mu\text{m cm}/(\text{V s})$)
ARLINs	-16.3 ± 0.4	-1.3 ± 0.1
doxorubicin-encapsulated ARLINs	-17.8 ± 1.3	-1.4 ± 0.1

Table 2. Effect of Gel Filtration on Physical Properties of ARLINs Determined Using Dynamic Light Scattering Method ($n = 5$)

	hydrodynamic diameter (nm)	zeta potential (mV)	electrophoretic mobility ($\mu\text{m cm}/(\text{V s})$)
before gel filtration	147.1 ± 12.7	-18.0 ± 0.5	-1.4 ± 0.1
after gel filtration	158.3 ± 8.1	-17.8 ± 1.3	-1.5 ± 0.1

harmonic (at twice the excitation frequency, 7 MHz). The control data indicates the response without any ARLINs in suspension. There was an enhancement in response for both components that demonstrates the echogenic nature of the ARLINs. The fundamental response shows around 20 dB enhancement for the lipid concentration of 5 $\mu\text{g}/\text{mL}$ at an acoustic pressure of 500 kPa. The nonlinear response from the

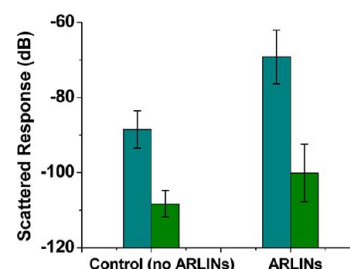


Figure 6. In vitro ultrasound scattering: fundamental (dark cyan) and second harmonic (green) responses from ARLINs ($n = 5$).

ARLINs is much weaker with only 8 dB enhancement for the second harmonic component. Note that normal ELIPs⁴¹ and our previously reported lipopeptide conjugated ELIPs generated larger (33 and 25 dB, respectively) enhancement of the fundamental response at 10 $\mu\text{g}/\text{mL}$ (double the concentration accounts for 3 dB discrepancy) lipid concentration and 500 kPa. The weaker response here may be attributed to the change in the lipid composition and increased strength of lipid shell due to polymerization. Note that as reported previously^{30,41} with other ELIPs, scattered responses from lipopeptide incorporated ELIPs do not show any distinct peak at the subharmonic frequency (at half the excitation frequency or 1.75 MHz). Echogenicity was also confirmed by ultrasound imaging with a Terason t3200 ultrasonic medical

imaging system using a 4–15 MHz transducer. Reconstituted ARLINs reflected ultrasound, indicating the presence of entrapped air inside (Figure 7B), whereas control samples (no ARLINs) were dark due to no reflection (Figure 7A).

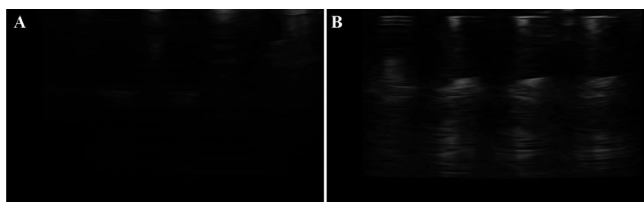


Figure 7. Ultrasound imaging of ARLINs reconstituted in 10 mM HEPES buffer pH 7.4, using a Terason t3200 ultrasonic medical imaging system using a 12–15 MHz transducer. (A) Control: 10 mM HEPES buffer pH 7.4; (B) ARLINs sample: 0.1 mg/mL.

We encapsulated the dye calcein in the aqueous interior of the ARLINs and added cobalt(II) chloride (CoCl_2) in the outside buffer. Most of the triggered release reports from drug carriers containing disulfide bonds employ either dithiothreitol (DTT⁶⁶) or cysteine (CYS⁶⁷) as the reducing agent. Hence, we decided to perform the release studies using DTT and CYS, as well as the physiologically more relevant reducing agent glutathione (GSH). Upon addition of the reducing agent, as the encapsulated calcein is released, its emission intensity is quenched by the CoCl_2 in the external media.

We studied the release of encapsulated calcein from the ARLINs using 10 μM to 10 mM concentrations of reducing agents. The range was selected based on the concentrations of reducing agents in the extracellular matrix/blood plasma (10 μM) and cancer cell cytosol (10 mM). The disulfide bonds on the external surface of the ARLINs were cleaved (disulfide to thiol exchange) by the added reducing agents. This process creates sufficient disturbance to make nanoparticles unstable and leaky. We observed that the percent release was directly proportional to the concentration of reducing agents (Figure 8A). The maximum release of around 90% was observed with 10 mM concentration of either GSH or DTT.

DTT has a very low redox potential ($E_0 = -0.332$ V at pH 7.0) and it rapidly reduces the disulfide bonds⁶⁸ as compared to glutathione ($E_0 = +0.062$ V) and cysteine ($E_0 = +0.025$ V).^{69,70} In fact, DTT reduces the bonds so rapidly that we were unable to obtain a reliable release profile from the ARLINs. However,

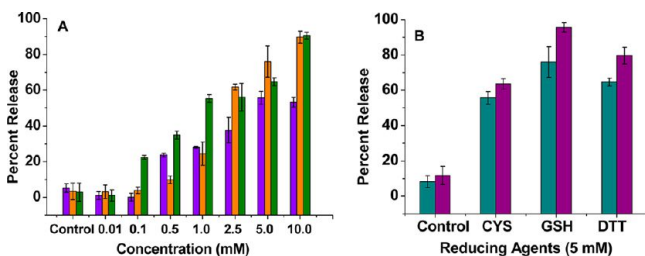


Figure 8. (A) Thiol-triggered release of calcein from polymer-coated ARLINs with increasing concentration of reducing agents CYS (violet), GSH (orange), and DTT (green). (B) Ultrasound enhancement of redox-triggered release from ARLINs. The dark cyan columns indicate release with reducing agents at 5 mM concentration and violet columns indicate release with simultaneous application of two triggers: reducing agent (5 mM) and ultrasound (CW excitation at 3 MHz, 0.5 MPa for 2 min; $n = 5$).

the release profiles employing GSH and CYS were slow enough to be easily analyzed (Figure 9). Given the relative

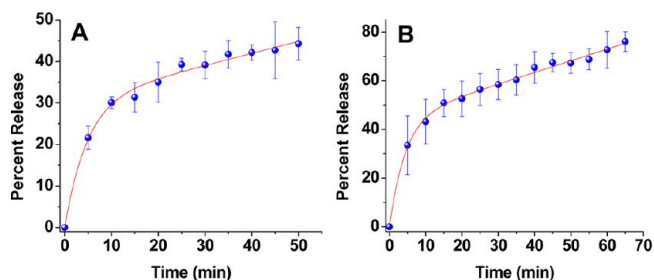


Figure 9. Release profiles of calcein from ARLINs in presence of 5 mM CYS (A) and 5 mM GSH (B). The red lines indicate the fitted curves for the observed data using the eq 1 ($n = 3$).

concentrations of reducible disulfide bonds and reducing agents, we expected the overall kinetic profile to be single exponential in nature. The latter was found to be the case for the release of the encapsulated content from photocleavable as well as enzyme (MMP-9) cleavable liposomes,⁵ albeit in both these cases the single exponential phases proceeded with a finite lag phase. No lag phase was noticeable during the GSH- and CYS-dependent cleavage of these ARLINs. However, in attempting to analyze the data of Figure 9, we realized that the release profile did not conform to the single exponential rate equation. The data could only be fitted by the single exponential plus steady-state equation in the following format (eq 1).

$$\text{release} = F_1(1 - e^{-k_1 t}) + k_2 t + \text{offset} \quad (1)$$

where k_1 and k_2 are the rate constants of exponential and steady-state phases. The solid lines in Figure 9 are the best fitted curves of the data. We determined the magnitudes of k_1 to be $0.21 \pm 0.03 \text{ min}^{-1}$ (for CYS-mediated release) and $0.23 \pm 0.02 \text{ min}^{-1}$ (for GSH-mediated release); the values for k_2 being equal to 0.18 ± 0.01 (for CYS-mediated release) and $0.25 \pm 0.01 \text{ min}^{-1}$ (for GSH-mediated release).

The question arose as to why, unlike other formulations,⁴ the thiol-mediated cleavage and content release from disulfide-linked ARLINs exhibited the single exponential (burst) phase followed by the steady-state phase. In contemplating the mechanistic origin of such a profile (Figure 9), we realized that due to initial high concentration of GSH and CYS, they would rapidly reduce a major fraction of the disulfide bonds of the ARLINs. Subsequently, the reducing agent (e.g., CYS or GSH) as well as the reduced thiol groups on the ARLINs surface would trigger the sulfhydryl-disulfide exchange reaction in a steady-state fashion. Such a situation is unlikely to prevail either with photo- or MMP-9 cleavable drug carriers, and thus, the release profiles are devoid of the steady-state phase. We are currently assessing the molecular mechanism underlying the release of contents under different experimental conditions to validate or refute our working hypothesis, and we will report our findings subsequently.

We observed minimal leakage (less than 5% over 12 h at room temperature in pH 7.4 buffer) from the ARLINs in the absence of any added reducing agent (Figure 8A). With 10 μM concentration of the reducing agents, the release was less than 5% – indicating the relative stability of ARLINs in extracellular environments/bloodstream. This is likely due to the polymerized external leaflet of the ARLINs. We note that the

extracellular environment of tumors is more reducing compared normal cells (because of cell deaths, necrosis) and this can lead to release of some of the encapsulated contents from the ARLINs.

DTT is a chelating agent and forms complexes with many transition metals ions.⁴³ We added 10 mM CoCl₂ in the buffer to quench the fluorescence emission from the calcein released from the ARLINs. It is likely that a considerable amount of DTT is consumed in forming complexes with the added Co²⁺ ions. This will likely contribute to lesser release from the ARLINs in presence of 5 mM DTT as compared to 5 mM GSH. We also observed and confirmed that DTT results in the highest amount of complex formation and precipitation, followed by CYS. The formation of colored complex and precipitate were minimal with GSH.

It was evident from the in vitro scattering experiments, TEM images, and ultrasound imaging that these lipid nanoparticles were echogenic and contains entrapped air inside. After ensuring release with reducing agents, we proceeded to determine whether the ARLINs release calcein in response to an ultrasound trigger. In this endeavor, reconstituted ARLINs along with CoCl₂ were taken in the wells of a 48 well plate and excited with continuous wave ultrasound. We observed that in absence of any reducing agents, ultrasound alone failed to release calcein from ARLINs. Less than 5% release was observed in both control and test samples containing less than 0.5 mM of reducing agents after application of continuous wave ultrasonic excitation (3 MHz frequency, 0.5 MPa acoustic pressure for 2 min). Increasing the intensity of ultrasound to higher values had no significant effect on the results. Subsequently, we added 5 mM reducing agents to ARLINs and applied ultrasound concurrently to observe the combined effects of both triggers on the release. With simultaneous application of both triggers, 8–20% enhancement in release was observed as compared to release with reducing agents alone. ARLINs treated with GSH showed the highest additional enhancement (20%) with ultrasound trigger, whereas CYS-treated sample showed only 8% additional ultrasound induced enhancement under the same excitation conditions. We note that GSH is more effective in reducing the disulfide groups on ARLIN surface and release more contents compared to CYS (Figure 9).

In another set of experiments, ultrasonic excitation was initiated an hour after incubating ARLINs with the reducing agents (5 mM). No significant change in calcein release was observed. We hypothesize that, upon incubating ARLINs with reducing agents for an hour, the lipid shell of nanoparticle becomes leaky, allowing the entrapped air to escape, thereby diminishing their acoustic reflectivity.

These observations suggest that polymerization on the external surface makes lipid shell stronger and less responsive to disturbance created by ultrasound excitation of air entrapped inside. Hence, ultrasound alone fails to create a sufficient disturbance or defects in the polymer-coated lipid shell in order to release calcein from its aqueous core. But once reducing agents are added, the effects of polymerization are reversed, making ARLINs sensitive to ultrasound and release the contents. This further corroborates our hypothesis that cross-linking/polymerization using reversible disulfide bonds leads to stronger and more stable ARLINs without compromising release efficacy at targeted sites (reducing environment of cell cytosol). This hypothesis was also supported by the release data obtained upon application of low frequency ultrasound (CW,

22.5 kHz, 4 W, usually applied to disrupt cell membranes) to nonpolymerized and polymerized ARLINs (Figure 10). The obtained results clearly show that, at each time interval, the release was less with polymer-coated ARLINs compared to nonpolymerized ARLINs.

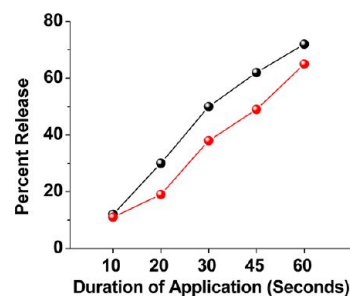


Figure 10. Low frequency ultrasound (CW, 22.5 kHz, 4W) triggered release from ARLINs prior to polymerization (black spheres) and after polymerization (red spheres).

Subsequently, we proceeded to demonstrate the effectiveness of our ARLINs in releasing the encapsulated contents in the cytosol of cancer cells. In this endeavor, we used folic acid as the targeting group for the ARLINs. Folic acid is a vitamin B family member which plays an important role in cell survival by participating in the biosynthesis of nucleic acids and amino acids.⁷¹ Due to the faster growth rate, cancer cells need more folic acid compared to normal cells. As a result, cancer cells express higher number of folic acid receptors on the surface compared to normal cells. Folate receptors actively internalize bound folic acid or folate conjugated entities via receptor mediated endocytosis.^{72,73} Folate conjugation to anticancer drugs or delivery vehicles improves drug selectivity for cancer cells overexpressing the folate receptor on the surface.^{74–79}

For the cellular studies, we incorporated the DPPE-PEG₂₀₀₀-folate lipid (Figure 2, 1 mol %) in the ARLINs and studied their uptake by folate overexpressing breast cancer cell line MCF-7. For these experiments, the nontargeted ARLINs were used as the controls. MCF-7 is a breast cancer cell line known to overexpress folate receptors and has been used to demonstrate enhanced uptake of folate-conjugated, drug delivery systems.^{80–84} We observed significantly higher uptake of folate-lipid incorporated ARLINs in the MCF-7 cells compared to the nontargeted ARLINs. There was a significant difference in calcein fluorescence observed in confocal fluorescence microscopic images (at 10 and 20 min) of folate conjugated ARLINs compared to the nontargeted ARLINs (Figure 11). We observed that maximum uptake of the folate incorporated ARLINs in the MCF-7 cells takes place after 20 min of incubation. We also studied the release kinetics of these ARLINs (0.02 mg/mL) incubated in human serum and the dye-free cell culture media (RPMI) for an hour. We noticed that, in these experiments, the ARLINs leaked less than 5% of the encapsulated dye in 1 h.

We further determined the percent uptake of the ARLINs uptake by the cells. In this endeavor, the MCF-7 cells were incubated with two different concentrations of ARLINs (40 and 20 µg/mL) encapsulating 50 mM calcein for 6 h. Subsequently, the cell were washed with HBSS and disrupted by the addition of 5% Triton X-100 solution. The ARLINs were also disrupted using 5% Triton-X100 solution. The fluorescence emission intensity for the calcein were measured for both samples and

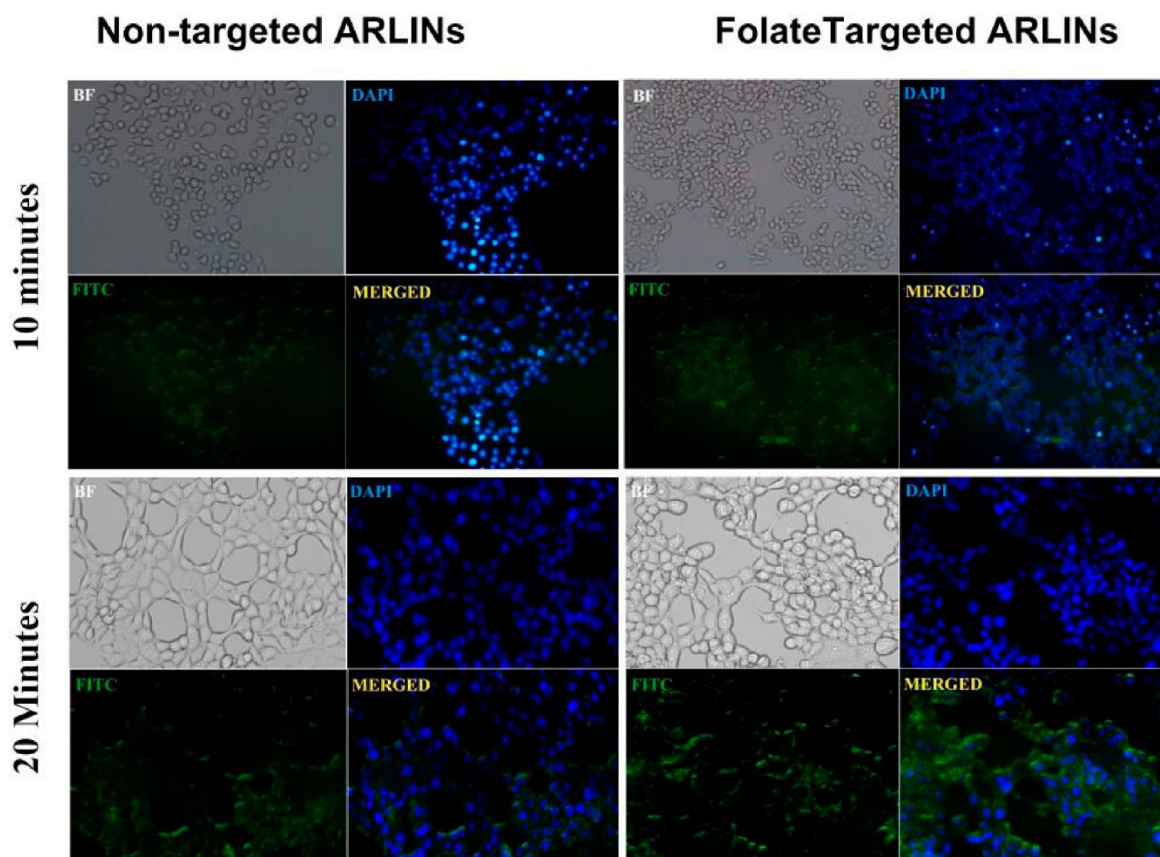


Figure 11. Fluorescence microscopic images of ARLINs uptake by folate receptor overexpressing MCF-7 cancer cell line (20× magnification).

the percent uptake was calculated accordingly. We observed that the folate-targeted ARLINs were taken up by MCF-7 cells in higher amount compared to nontargeted ARLINs (Figure 12

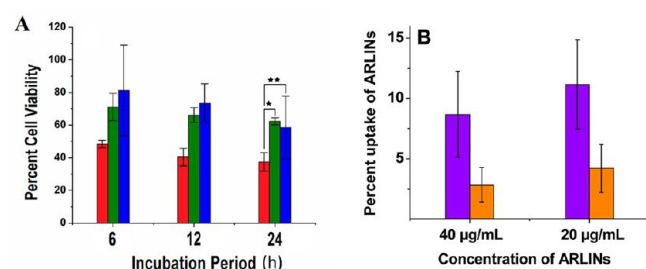


Figure 12. (A) Cell viability studies with HeLa cells: folate-conjugated, doxorubicin-loaded ARLINs (red), nontargeted, doxorubicin-loaded ARLINs (green), and free doxorubicin (blue). The final doxorubicin concentration used was 50 µg/mL in all the samples ($n = 6$); $*P < 0.001$ $**P < 0.05$. (B) Percent uptake of folate-targeted (violet bars) and nontargeted (orange bars) ARLINs by the MCF-7 cells after incubation for 6 h.

B). This result corroborates the confocal microscopic images obtained with the targeted and nontargeted ARLINs with the MCF-7 cells (Figure 11). We observed that uptake was slow; 6 h incubation led to around 10% uptake with folate-targeted ARLINs (Figure 12B). We also observed that uptake was concentration-dependent, percent uptake increased with a decrease in concentration, but the total uptake increases with an increase in concentration of ARLINs.

Subsequently, we encapsulated the anticancer drug doxorubicin in the folate-PEG lipid incorporated ARLINs by pH gradient method (80–90% encapsulation efficiency). Although some leakage of doxorubicin was observed during polymerization, we found that cell viability decreases to 37% when folate-conjugated, doxorubicin-encapsulated ARLINs were incubated with HeLa cells (human cervical carcinoma overexpressing folate receptors) for 24 h. The cell viability was significantly lower for folate-conjugated ARLINs compared to nontargeted ARLINs ($p < 0.001$) and free doxorubicin ($p < 0.05$), indicating that folate conjugation enhances the uptake in the HeLa cells (Figure 12B). This was further confirmed by capturing fluorescence microscopic images of HeLa cells incubated with doxorubicin-ARLINs. The images clearly show enhanced uptake of doxorubicin-loaded-ARLINs into the cytosol of the HeLa cells (Figure 13).

CONCLUSIONS

We have successfully demonstrated the preparation of polymer-coated ARLINs. These lipid nanoparticles were stable in the extracellular oxidizing environment but released their contents efficiently in the reducing environment of cell cytosol. The ARLINs were also found to be echogenic with a 20 dB enhancement in fundamental scattered response with 3.5 MHz excitation at 500 kPa acoustic pressure for a lipid concentration of 5 µg/mL. Although the ARLINs failed to show significant release under diagnostic frequency ultrasonic excitation alone, the release was enhanced by simultaneous application of ultrasound and redox triggers. Doxorubicin-loaded ARLINs showed enhanced uptake and cytotoxicity when conjugated to

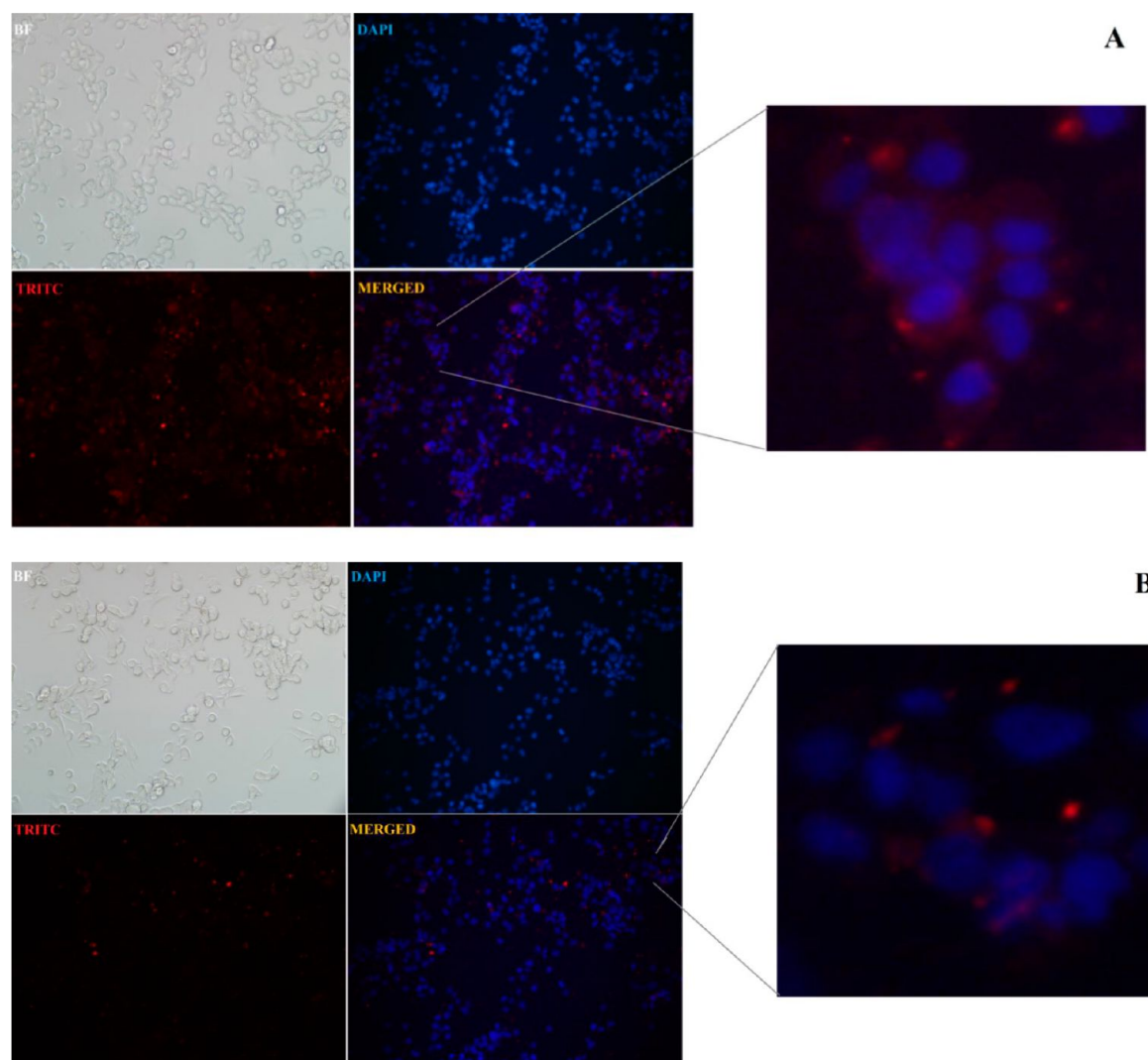


Figure 13. Fluorescence microscopic images for the uptake of doxorubicin loaded ARLINs by folate receptor overexpressing HeLa cells. (A) Folate-conjugated, doxorubicin-loaded ARLINs; (B) nontargeted, doxorubicin-loaded ARLINs (20× magnification).

folic acid and thus can be used for targeted drug delivery for cancer cells overexpressing folate receptors on their surface. We have employed continuous wave ultrasound excitation for release studies, which sends more energy than pulsed ultrasound. Future studies are needed to optimize the ultrasound parameters such as frequency, intensity, and duty cycles to establish optimum parameters maximum possible release. The current study, however, successfully validates the proof of concept and with further developments and modifications, these polymer-coated ARLINs have the potential to be used as multimodal nanocarriers for targeted drug delivery, and simultaneous ultrasound imaging.

■ AUTHOR INFORMATION

Corresponding Author

*Tel.: 701-231-7888. Fax: 701-231-8333. E-mail: sanku.mallik@ndsus.edu.

Notes

The authors declare no competing financial interest.

■ ACKNOWLEDGMENTS

This research was supported by NIH Grants 1R01 CA 113746, 1R01 CA 132034 to S.M. and D.K.S., NSF Grant DMR 1005011 to S.M. and DMR-1005283, NIH Grant P20RR016472 to K.S. We thank Prof. Christy K. Holland and Jonathan Kopechek (Department of Internal Medicine, University of Cincinnati) for helpful discussions. We thank Prof. Subbaraya Yuvarajan (Department of Electrical Engineering, North Dakota State University) for calibrating the amplifier for the ultrasound experiments.

■ REFERENCES

- (1) Bhattacharjee, H.; Balabathula, P.; Wood, G. C. Targeted nanoparticulate drug-delivery systems for treatment of solid tumors: a review. *Ther. Delivery* **2010**, *1* (5), 713–34.
- (2) Barenholz, Y. C. Doxil(R) - The first FDA-approved nano-drug: Lessons learned. *J. Controlled Release* **2012**, *160* (2), 117–34.
- (3) Gordon, K. B.; Tajuddin, A.; Guitart, J.; Kuzel, T. M.; Eramo, L. R.; VonRoenn, J. Hand-foot syndrome associated with liposome-encapsulated doxorubicin therapy. *Cancer* **1995**, *75* (8), 2169–73.
- (4) Banerjee, J.; Hanson, A. J.; Gadani, B.; Elegbede, A. I.; Tobwala, S.; Ganguly, B.; Wagh, A. V.; Muhonen, W. W.; Law, B.; Shabb, J. B.; Srivastava, D. K.; Mallik, S. Release of liposomal contents by cell-

secreted matrix metalloproteinase-9. *Bioconjugate Chem.* **2009**, *20* (7), 1332–9.

(5) Sarkar, N.; Banerjee, J.; Hanson, A. J.; Elegbede, A. I.; Rosendahl, T.; Krueger, A. B.; Banerjee, A. L.; Tobwala, S.; Wang, R.; Lu, X.; Mallik, S.; Srivastava, D. K. Matrix metalloproteinase-assisted triggered release of liposomal contents. *Bioconjugate Chem.* **2008**, *19* (1), 57–64.

(6) Ong, W.; Yang, Y.; Cruciano, A. C.; McCarley, R. L. Redox-triggered contents release from liposomes. *J. Am. Chem. Soc.* **2008**, *130* (44), 14739–44.

(7) Hu, F. Q.; Zhang, Y. Y.; You, J.; Yuan, H.; Du, Y. Z. pH triggered doxorubicin delivery of PEGylated glycolipid conjugate micelles for tumor targeting therapy. *Mol. Pharm.* **2012**, *9* (9), 2469–78.

(8) Turner, D. C.; Moshkelani, D.; Shemesh, C. S.; Luc, D.; Zhang, H. Near-infrared image-guided delivery and controlled release using optimized thermosensitive liposomes. *Pharm. Res.* **2012**, *29* (8), 2092–103.

(9) Leung, S. J.; Kachur, X. M.; Bobnick, M. C.; Romanowski, M. Wavelength-selective light-induced release from plasmon resonant liposomes. *Adv. Funct. Mater.* **2011**, *21* (6), 1113–1121.

(10) Smith, D. A.; Vaidya, S. S.; Kopeček, J. A.; Huang, S. L.; Klegerman, M. E.; McPherson, D. D.; Holland, C. K. Ultrasound-triggered release of recombinant tissue-type plasminogen activator from echogenic liposomes. *Ultrasound Med. Biol.* **2010**, *36* (1), 145–57.

(11) Melancon, M. P.; Zhou, M.; Li, C. Cancer theranostics with near-infrared light-activatable multimodal nanoparticles. *Acc. Chem. Res.* **2011**, *44* (10), 947–56.

(12) Sciallero, C.; Paradossi, G.; Trucco, A. A preliminary in vitro assessment of polymer-shelled microbubbles in contrast-enhanced ultrasound imaging. *Ultrasonics* **2012**, *52* (3), 456–64.

(13) Mohan, P.; Rapoport, N. Doxorubicin as a molecular nanotheranostic agent: effect of doxorubicin encapsulation in micelles or nanoemulsions on the ultrasound-mediated intracellular delivery and nuclear trafficking. *Mol. Pharm.* **2010**, *7* (6), 1959–73.

(14) Tang, S. Y.; Sivakumar, M.; Ng, A. M.; Shridharan, P. Anti-inflammatory and analgesic activity of novel oral aspirin-loaded nanoemulsion and nano multiple emulsion formulations generated using ultrasound cavitation. *Int. J. Pharm.* **2012**, *430* (1–2), 299–306.

(15) Thirumalai, S.; Mobed-Miremadi, M.; Sridhar-Keralapura, M. *IEEE Eng. Med. Biol. Soc.* **2011**, 7207–10.

(16) Min, H. S.; Kang, E.; Koo, H.; Lee, J.; Kim, K.; Park, R. W.; Kim, I. S.; Choi, Y.; Kwon, I. C.; Han, M. Gas-generating polymeric microspheres for long-term and continuous in vivo ultrasound imaging. *Biomaterials* **2012**, *33* (3), 936–44.

(17) Huang, S. L.; Hamilton, A. J.; Nagaraj, A.; Tiukinhoy, S. D.; Klegerman, M. E.; McPherson, D. D.; MacDonald, R. C. Improving ultrasound reflectivity and stability of echogenic liposomal dispersions for use as targeted ultrasound contrast agents. *J. Pharm. Sci.* **2001**, *90* (12), 1917–1926.

(18) Wrenn, S.; Dicker, S.; Small, E.; Mleczko, M. Controlling cavitation for controlled release. In *Ultrasonics Symposium (IUS)*, 2009 IEEE International, Roma, Italy, 20–23 Sept. 2009, pp 104–107.

(19) Schroeder, A.; Avnir, Y.; Weisman, S.; Najajreh, Y.; Gabizon, A.; Talmon, Y.; Kost, J.; Barenholz, Y. Controlling liposomal drug release with low frequency ultrasound: Mechanism and feasibility. *Langmuir* **2007**, *23* (7), 4019–4025.

(20) Schroeder, A.; Kost, J.; Barenholz, Y. Ultrasound, liposomes, and drug delivery: principles for using ultrasound to control the release of drugs from liposomes. *Chem. Phys. Lipids* **2009**, *162* (1–2), 1–16.

(21) Negishi, Y.; Matsuo, K.; Endo-Takahashi, Y.; Suzuki, K.; Matsuki, Y.; Takagi, N.; Suzuki, R.; Maruyama, K.; Aramaki, Y. Delivery of an angiogenic gene into ischemic muscle by novel bubble liposomes followed by ultrasound exposure. *Pharm. Res.* **2011**, *28* (4), 712–719.

(22) Evjen, T. J.; Nilssen, E. A.; Rognvaldsson, S.; Brandl, M.; Fossheim, S. L. Distearoylphosphatidylethanolamine-based liposomes for ultrasound-mediated drug delivery. *Eur. J. Pharm. Biopharm.* **2010**, *75* (3), 327–33.

(23) Pong, M.; Umchid, S.; Guarino, A. J.; Lewin, P. A.; Litniewski, J.; Nowicki, A.; Wrenn, S. P. In vitro ultrasound-mediated leakage from phospholipid vesicles. *Ultrasonics* **2006**, *45* (1–4), 133–145.

(24) Lin, H. Y.; Thomas, J. L. Factors affecting responsivity of unilamellar liposomes to 20 kHz ultrasound. *Langmuir* **2004**, *20* (15), 6100–6.

(25) Lin, H. Y.; Thomas, J. L. PEG-Lipids and oligo(ethylene glycol) surfactants enhance the ultrasonic permeabilizability of liposomes. *Langmuir* **2003**, *19* (4), 1098–1105.

(26) Husseini, G. A.; Myrup, G. D.; Pitt, W. G.; Christensen, D. A.; Rapoport, N. A. Y. Factors affecting acoustically triggered release of drugs from polymeric micelles. *J. Controlled Release* **2000**, *69* (1), 43–52.

(27) Kopeček, J. A.; Abruzzo, T. M.; Wang, B.; Chrzanowski, S. M.; Smith, D. A.; Kee, P. H.; Huang, S.; Collier, J. H.; McPherson, D. D.; Holland, C. K. Ultrasound-mediated release of hydrophilic and lipophilic agents from echogenic liposomes. *J. Ultrasound Med.* **2008**, *27* (11), 1597–606.

(28) Buchanan, K. D.; Huang, S. L.; Kim, H.; McPherson, D. D.; MacDonald, R. C. Encapsulation of NF-kappaB decoy oligonucleotides within echogenic liposomes and ultrasound-triggered release. *J. Controlled Release* **2010**, *141* (2), 193–8.

(29) Herbst, S. M.; Klegerman, M. E.; Kim, H.; Qi, J.; Shelat, H.; Wassler, M.; Moody, M. R.; Yang, C. M.; Ge, X.; Zou, Y.; Kopeček, J. A.; Clubb, F. J.; Kraemer, D. C.; Huang, S.; Holland, C. K.; McPherson, D. D.; Geng, Y. J. Delivery of stem cells to porcine arterial wall with echogenic liposomes conjugated to antibodies against CD34 and intercellular adhesion molecule-1. *Mol. Pharm.* **2010**, *7* (1), 3–11.

(30) Nahire, R.; Paul, S.; Scott, M. D.; Singh, R. K.; Muhonen, W. W.; Shabb, J.; Gange, K. N.; Srivastava, D. K.; Sarkar, K.; Mallik, S. Ultrasound enhanced matrix metalloproteinase-9 triggered release of contents from echogenic liposomes. *Mol. Pharm.* **2012**, *9* (9), 2554–64.

(31) Kheiriloom, A.; Dayton, P. A.; Lum, A. F. H.; Little, E.; Paoli, E. E.; Zheng, H. R.; Ferrara, K. W. Acoustically-active microbubbles conjugated to liposomes: Characterization of a proposed drug delivery vehicle. *J. Controlled Release* **2007**, *118* (3), 275–284.

(32) Huang, S. L.; Hamilton, A. J.; Nagaraj, A.; Tiukinhoy, S. D.; Klegerman, M. E.; McPherson, D. D.; MacDonald, R. C. Improving ultrasound reflectivity and stability of echogenic liposomal dispersions for use as targeted ultrasound contrast agents. *J. Pharm. Sci.* **2001**, *90* (12), 1917–26.

(33) Huang, S. L.; McPherson, D. D.; MacDonald, R. C. A method to co-encapsulate gas and drugs in liposomes for ultrasound-controlled drug delivery. *Ultrasound Med. Biol.* **2008**, *34* (8), 1272–80.

(34) Alkan-Onyuksel, H.; Demos, S. M.; Lanza, G. M.; Vonesh, M. J.; Klegerman, M. E.; Kane, B. J.; Kuszak, J.; McPherson, D. D. Development of inherently echogenic liposomes as an ultrasonic contrast agent. *J. Pharm. Sci.* **1996**, *85* (5), 486–90.

(35) Omata, D.; Negishi, Y.; Hagiwara, S.; Yamamura, S.; Endo-Takahashi, Y.; Suzuki, R.; Maruyama, K.; Aramaki, Y. Enhanced gene delivery using Bubble liposomes and ultrasound for folate-PEG liposomes. *J. Drug Targeting* **2012**, *20* (4), 355–63.

(36) Omata, D.; Negishi, Y.; Yamamura, S.; Hagiwara, S.; Endo-Takahashi, Y.; Suzuki, R.; Maruyama, K.; Nomizu, M.; Aramaki, Y. Involvement of Ca(2)(+) and ATP in enhanced gene delivery by bubble liposomes and ultrasound exposure. *Mol. Pharm.* **2012**, *9* (4), 1017–23.

(37) Waseda, K.; Ako, J.; Yamasaki, M.; Koizumi, T.; Ormiston, J.; Worthley, S. G.; Whitbourn, R. J.; Walters, D. L.; Honda, Y.; Meredith, I. T.; Fitzgerald, P. J. Short- and mid-term intravascular ultrasound analysis of the new zotarolimus-eluting stent with durable polymer - results from the RESOLUTE trial. *Circ. J.* **2010**, *74* (10), 2097–102.

(38) Laing, S. T.; Moody, M.; Smulevitz, B.; Kim, H.; Kee, P.; Huang, S.; Holland, C. K.; McPherson, D. D. Ultrasound-enhanced thrombolytic effect of tissue plasminogen activator-loaded echogenic liposomes in an in vivo rabbit aorta thrombus model—brief report. *Arterioscler., Thromb., Vasc. Biol.* **2011**, *31* (6), 1357–9.

- (39) Huang, S. L. Liposomes in ultrasonic drug and gene delivery. *Adv. Drug Delivery Rev.* **2008**, *60* (10), 1167–1176.
- (40) Kopeček, J. A.; Haworth, K. J.; Raymond, J. L.; Mast, T. D.; Perrin, S. R.; Klegerman, M. E.; Huang, S. L.; Porter, T. M.; McPherson, D. D.; Holland, C. K. Acoustic characterization of echogenic liposomes: Frequency-dependent attenuation and backscatter. *J. Acoust. Soc. Am.* **2011**, *130* (5), 3472–3481.
- (41) Paul, S.; Russakow, D.; Nahire, R.; Nandy, T.; Ambre, A. H.; Katti, K.; Mallik, S.; Sarkar, K. In vitro measurement of attenuation and nonlinear scattering from echogenic liposomes. *Ultrasonics* **2012**, *52* (7), 962–9.
- (42) Kopeček, J. A.; Haworth, K. J.; Raymond, J. L.; Douglas Mast, T.; Perrin, S. R.; Klegerman, M. E.; Huang, S.; Porter, T. M.; McPherson, D. D.; Holland, C. K. Acoustic characterization of echogenic liposomes: frequency-dependent attenuation and backscatter. *J. Acoust. Soc. Am.* **2011**, *130* (5), 3472–81.
- (43) Kr zel, A.; Lesniak, W.; Jezowska-Bojczuk, M.; Mlynarz, P.; Brasun, J.; Kozłowski, H.; Bal, W. Coordination of heavy metals by dithiothreitol, a commonly used thiol group protectant. *J. Inorg. Biochem.* **2001**, *84* (1–2), 77–88.
- (44) Huang, S. L.; MacDonald, R. C. Acoustically active liposomes for drug encapsulation and ultrasound-triggered release. *Biochim. Biophys. Acta* **2004**, *1665* (1–2), 134–41.
- (45) Hub, H. H.; Hupfer, B.; Koch, H.; Ringsdorf, H. Polymerizable phospholipid analogues—new stable biomembrane and cell models. *Angew. Chem., Int. Ed.* **1980**, *19* (11), 938–40.
- (46) Raderer, M.; Scheithauer, W. Clinical trials of agents that reverse multidrug resistance. A literature review. *Cancer* **1993**, *72* (12), 3553–63.
- (47) Perry, R. R.; Mazetta, J. A.; Levin, M.; Barranco, S. C. Glutathione levels and variability in breast tumors and normal tissue. *Cancer* **1993**, *72* (3), 783–7.
- (48) Berger, S. J.; Gosky, D.; Zborowska, E.; Willson, J. K.; Berger, N. A. Sensitive enzymatic cycling assay for glutathione: measurements of glutathione content and its modulation by buthionine sulfoximine in vivo and in vitro in human colon cancer. *Cancer Res.* **1994**, *54* (15), 4077–83.
- (49) Cook, J. A.; Pass, H. I.; Iype, S. N.; Friedman, N.; DeGraff, W.; Russo, A.; Mitchell, J. B. Cellular glutathione and thiol measurements from surgically resected human lung tumor and normal lung tissue. *Cancer Res.* **1991**, *51* (16), 4287–94.
- (50) Joncourt, F.; Oberli-Schrammli, A. E.; Stadler, M.; Buser, K.; Franscini, L.; Fey, M. F.; Cerny, T. Patterns of drug resistance parameters in adult leukemia. *Leuk. Lymphoma* **1995**, *17* (1–2), 101–9.
- (51) Mulder, T. P.; Manni, J. J.; Roelofs, H. M.; Peters, W. H.; Wiersma, A. Glutathione S-transferases and glutathione in human head and neck cancer. *Carcinogenesis* **1995**, *16* (3), 619–24.
- (52) Cotgreave, I. A.; Gerdes, R. G. Recent trends in glutathione biochemistry—glutathione-protein interactions: a molecular link between oxidative stress and cell proliferation? *Biochem. Biophys. Res. Commun.* **1998**, *242* (1), 1–9.
- (53) Saito, G.; Swanson, J. A.; Lee, K. D. Drug delivery strategy utilizing conjugation via reversible disulfide linkages: role and site of cellular reducing activities. *Adv. Drug Delivery Rev.* **2003**, *55* (2), 199–215.
- (54) West, K. R.; Otto, S. Reversible covalent chemistry in drug delivery. *Curr. Drug Discovery Technol.* **2005**, *2* (3), 123–60.
- (55) Goldenbogen, B.; Brodersen, N.; Gramatica, A.; Loew, M.; Liebscher, J.; Herrmann, A.; Egger, H.; Budde, B.; Arbužova, A. Reduction-sensitive liposomes from a multifunctional lipid conjugate and natural phospholipids: reduction and release kinetics and cellular uptake. *Langmuir* **2011**, *27* (17), 10820–9.
- (56) Cho, H.; Bae, J.; Garripelli, V. K.; Anderson, J. M.; Jun, H. W.; Jo, S. Redox-sensitive polymeric nanoparticles for drug delivery. *Chem Commun (Cambridge, U.K.)* **2012**, *48*, 6043–45.
- (57) Graf, N.; Lippard, S. J. Redox activation of metal-based prodrugs as a strategy for drug delivery. *Adv. Drug Delivery Rev.* **2012**, *64* (11), 993–1004.
- (58) Wen, H.; Dong, C.; Dong, H.; Shen, A.; Xia, W.; Cai, X.; Song, Y.; Li, X.; Li, Y.; Shi, D. Engineered redox-responsive PEG detachment mechanism in PEGylated nano-graphene oxide for intracellular drug delivery. *Small* **2012**, *8* (5), 760–9.
- (59) Zhang, S.; Zhao, Y. Controlled release from cleavable polymerized liposomes upon redox and pH stimulation. *Bioconjugate Chem.* **2011**, *22* (4), 523–8.
- (60) Niu, G.; Cogburn, B.; Hughes, J. Preparation and characterization of doxorubicin liposomes. *Methods Mol. Biol.* **2010**, *624*, 211–9.
- (61) Kopeček, J. A.; Kim, H.; McPherson, D. D.; Holland, C. K. Calibration of the 1-MHz Sonitron ultrasound system. *Ultrasound Med. Biol.* **2010**, *36* (10), 1762–6.
- (62) Hensel, K.; Mienkina, M. P.; Schmitz, G. Analysis of ultrasound fields in cell culture wells for in vitro ultrasound therapy experiments. *Ultrasound Med. Biol.* **2011**, *37* (12), 2105–15.
- (63) Albrecht, T.; Patel, N.; Cosgrove, D. O.; Jayaram, V.; Blomley, M. J.; Eckersley, R. Enhancement of power Doppler signals from breast lesions with the ultrasound contrast agent EchoGen emulsion: subjective and quantitative assessment. *Acad. Radiol.* **1998**, *5* (Suppl 1), S195–8 discussion S199.
- (64) Huang, S. L.; Hamilton, A. J.; Pozharski, E.; Nagaraj, A.; Klegerman, M. E.; McPherson, D. D.; MacDonald, R. C. Physical correlates of the ultrasonic reflectivity of lipid dispersions suitable as diagnostic contrast agents. *Ultrasound Med. Biol.* **2002**, *28* (3), 339–348.
- (65) Hitchcock, K. E.; Caudell, D. N.; Sutton, J. T.; Klegerman, M. E.; Vela, D.; Pyne-Geithman, G. J.; Abruzzo, T.; Cyr, P. E.; Geng, Y. J.; McPherson, D. D.; Holland, C. K. Ultrasound-enhanced delivery of targeted echogenic liposomes in a novel ex vivo mouse aorta model. *J. Controlled Release* **2010**, *144* (3), 288–95.
- (66) Li, X.; Zhao, Y. Protection/Deprotection of surface activity and its applications in the controlled release of liposomal contents. *Langmuir* **2012**, *28* (9), 4152–9.
- (67) Karathanasis, E.; Bhavane, R.; Annapragada, A. V. Triggered release of inhaled insulin from the agglomerated vesicles: pharmacodynamic studies in rats. *J. Controlled Release* **2006**, *113* (2), 117–27.
- (68) Cleland, W. W. Dithiothreitol, a New Protective Reagent for Sh Groups. *Biochemistry* **1964**, *3*, 480–2.
- (69) Tanaka, N.; Kolthoff, I. M.; Stricks, W. Oxidation of ferrous-cysteinate complex by cystine. Oxidation potential of the cystine-cysteine system. *J. Am. Chem. Soc.* **1955**, *77* (7), 2004–2006.
- (70) Green, D. E. The reduction potentials of cysteine, glutathione and glycylcysteine. *Biochem. J.* **1933**, *27* (3), 678–89.
- (71) Antony, A. C. Folate receptors. *Ann. Rev. Nutr.* **1996**, *16*, 501–21.
- (72) Kamen, B. A.; Capdevila, A. Receptor-mediated folate accumulation is regulated by the cellular folate content. *Proc. Natl. Acad. Sci. U.S.A.* **1986**, *83* (16), 5983–7.
- (73) Leamon, C. P.; Low, P. S. Delivery of macromolecules into living cells: a method that exploits folate receptor endocytosis. *Proc. Natl. Acad. Sci. U.S.A.* **1991**, *88* (13), 5572–6.
- (74) Soares, D. C.; Cardoso, V. N.; de Barros, A. L.; de Souza, C. M.; Cassali, G. D.; de Oliveira, M. C.; Ramaldes, G. A. Antitumoral activity and toxicity of PEG-coated and PEG-folate-coated pH-sensitive liposomes containing (1)(5)(9)Gd-DTPA-BMA in Ehrlich tumor bearing mice. *Eur. J. Pharm. Sci.* **2012**, *45* (1–2), 58–64.
- (75) Li, X.; Tian, X.; Zhang, J.; Zhao, X.; Chen, X.; Jiang, Y.; Wang, D.; Pan, W. In vitro and in vivo evaluation of folate receptor-targeting amphiphilic copolymer-modified liposomes loaded with docetaxel. *Int. J. Nanomed.* **2011**, *6*, 1167–84.
- (76) Li, H.; Piao, L.; Yu, B.; Yung, B. C.; Zhang, W.; Wang, P. G.; Lee, J. L.; Lee, R. J. Delivery of calf thymus DNA to tumor by folate receptor targeted cationic liposomes. *Biomaterials* **2011**, *32* (27), 6614–20.
- (77) Zhao, X. B.; Muthusamy, N.; Byrd, J. C.; Lee, R. J. Cholesterol as a bilayer anchor for PEGylation and targeting ligand in folate-receptor-targeted liposomes. *J. Pharm. Sci.* **2007**, *96* (9), 2424–35.
- (78) Gabizon, A.; Horowitz, A. T.; Goren, D.; Tzemach, D.; Shmeeda, H.; Zalipsky, S. In vivo fate of folate-targeted polyethylene-

glycol liposomes in tumor-bearing mice. *Clin. Cancer Res.* **2003**, *9* (17), 6551–9.

(79) Pan, X.; Lee, R. J. Tumour-selective drug delivery via folate receptor-targeted liposomes. *Expert Opin. Drug Delivery* **2004**, *1* (1), 7–17.

(80) Pan, J.; Feng, S. S. Targeting and imaging cancer cells by folate-decorated, quantum dots (QDs)- loaded nanoparticles of biodegradable polymers. *Biomaterials* **2009**, *30* (6), 1176–83.

(81) Lee, E. S.; Na, K.; Bae, Y. H. Doxorubicin loaded pH-sensitive polymeric micelles for reversal of resistant MCF-7 tumor. *J. Controlled Release* **2005**, *103* (2), 405–18.

(82) Lee, E. S.; Na, K.; Bae, Y. H. Polymeric micelle for tumor pH and folate-mediated targeting. *J. Controlled Release* **2003**, *91* (1–2), 103–13.

(83) Muthu, M. S.; Kulkarni, S. A.; Raju, A.; Feng, S. S. Theranostic liposomes of TPGS coating for targeted co-delivery of docetaxel and quantum dots. *Biomaterials* **2012**, *33* (12), 3494–501.

(84) Paolino, D.; Licciardi, M.; Celia, C.; Giammona, G.; Fresta, M.; Cavallaro, G. Folate-targeted supramolecular vesicular aggregates as a new frontier for effective anticancer treatment in in vivo model. *Eur. J. Pharm. Biopharm.* **2012**, *82* (1), 94–102.